POLITECNICO
MILANO 1863

Biophysical model of plant growth

A model for the evapotranspiration of the lettuce

Numerical Analysis Partial Differential Equations - 095964

Students:
Luca Ciarimboli
Lorenzo Citterio
Marianna Dell'Otto

Supervisors:
Prof. Simona Perotto
Nicola Ferro, *Ph.D.*
Ing. Alessandro Antona

Abstract

This report presents our project for "Numerical Analysis for PDEs" course. The project was proposed by Agricola Moderna, a start-up based in Melzo (MI) which grows crops using vertical farming techniques.
Our work aims to develop an integrated mathematical model for predicting the evapotranspiration of lettuce crops inside a cell of the vertical farm. Based only on previous research, the model merges simulations of air flow and heat transfer with evaluations of structural and non-structural dry weights to determine the Leaf Area Index (LAI) and latent heat exchange between crops and their environment. In particular, the main references of this project are: "Computational analysis of the environment in an indoor vertical farming system " by Naranjani B. et al. ([1]); "Validation of a Dynamic Lettuce Growth Model for Greenhouse Climate Control" by Van Henten E. J. ([2]); "Plant factories; crop transpiration and energy balance" by Graamans L. et al. ([3]).
As a result, we correctly obtained exponential growth of the lettuce mass and of the amount of water which is evapotranspired during an interval of 20 days. However, the numerical values obtained are not exactly the expected ones, yet they are reasonable enough under the assumptions that have been made. Also, the results obtained for the air velocity, pressure, temperature and H_2O and CO_2 species mass fractions within the cell are correct and behave as expected.
The report details the model's development, numerical discretization and implementation in FreeFem++, and presents simulation results supported by mesh convergence and error analysis, concluding with suggestions for future research. Both the mathematical model and its numerical implementation have been developed from scratch.

Contents

1 Introduction

Climate changes, with the resultant increase of the temperature and drought, and the growing global demand for food are becoming more and more impactful on traditional agriculture. Indeed, the scarcity of resources, such as soil fertility and irrigation water, and the environmental impact of conventional farming practices have driven the research for an alternative solution.
Unlike traditional methods, vertical farming involves cultivating crops in stacked layers in a controlled and protected environment, in such a way as to guarantee the production of resources even in the most inaccessible climatic conditions. This innovative approach maximizes space utilization - almost 98% of soil is saved - and enables year-round cultivation. Moreover, vertical farms optimize resources efficiency, reduce the need for harmful pesticides, and significantly lower transportation costs. On the other hand, maximal optimization of the resources, like energy and water, is crucial for economic sustainability of a vertical farm. In this field many researches and studies have been carried out along the last decade; in particular, in [1], a three-dimensional numerical model is developed to optimize air flow and heat transfer within an indoor system considering transpiration, carbon-dioxide consumption, and oxygen production; in [2] it is implemented a model to describe the behavior of the non-structural and the structural dry weight, as affected by the incident photosynthetically active radiation, the carbon dioxide concentration and the air temperature in a greenhouse; in [3] it is described a crop transpiration model that is able to determine the relation between sensible and latent heat exchange, as well as the corresponding vapour flux for the production of lettuce in closed systems.
The aim of this work, in collaboration with Agricola Moderna, is to find an overall mathematical model. Starting from the three studies above, it will merge the simulations of the air flow through the cell with the evaluation of the structural and non-structural dry weights, in order to obtain the latent heat exchange between the crop and the surrounding environment. In the first part, through Navier-Stokes equations, the air-flow is solved and the temperature is computed. Moreover, the CO_2 and H_2O mass fraction are obtained solving the corresponding partial differential equations (PDEs). These quantities serve as input for an ordinary differential equations (ODEs) system, from which the structural and non-structural dry weights of a seedling are evaluated to determinate the *Leaf Area Index* (LAI) and from this calculate the latent heat flux.
The work is structured as follows. In Section 2, the development of the mathematical model is detailed, with a particular care in highlighting all the assumption made and the physical interpretation of the equations. In Section 3, all the steps towards the numerical discretization are described. In Section 4, the numerical implementation of the model in a `FreeFem++` code is presented. `FreeFem++` is a 2D and 3D partial differential equations solver, based on `C++` language. The Navier-Stokes system is solved by the Newton's method, while the ODE system is discretized with a Crank-Nicholson scheme. Finally, in Section 5, we point out the results of our simulations supported by mesh convergence and error analysis. In the end, in Section 6, we conclude with some comments and potential further developments suggestions.

2 Mathematical Model

In this section, the mathematical model we have developed is illustrated in details. Here, before diving into the model description, the general idea is briefly outlined.
The aim is to develop an equation that provides a measure of the evapotranspiration, which represents the amount of water vapour that is released in the environment while the crop grows in time. Simply, in mathematical terms, this unknown variable of interest depends on the flux of latent heat coming from the crop's surface.
To reach this goal, we need to perform both an energy balance of the crop ([1]) and an energy balance of the whole cell ([3]). The interaction lettuce-air strongly depends on the crop growth in time. Indeed, it is clear that a newly planted crop and ready-to-be-harvested one have a different mass, volume, leaf surface and so on. Therefore, our model requires an evolution equation for the lettuce mass as well ([2]).

2.1 Air flow model

Here, we discuss a model suitable for the simulation of the air flow inside a cell. This is implemented through a system of PDEs including the Navier-Stokes equations, that allow us to compute the temperature in the cell. Moreover, we deduce the concentration of water and carbon dioxide through a mass fraction balance. These equations are essential to derive a growth model for the crop, as well as to perform a crop energy balance.

2.1.1 Navier-Stokes system

The energy balance equation is part of the Navier-Stokes (NS) system of equations for the air flow within the cell. The NS system of equations involves mass balance, momentum balance and energy balance. Here we start considering the first two.
Remark that, even if we stated above that we are looking for an evolution equation, in this section we are limiting ourselves to consider the steady-state NS system. This follows the fact that, as it will be shown in the numerical implementation, the advancement in time will appear only in the ODEs system for the crop's mass evolution. Hence, in the time-discretized model, we would just need to solve the steady-state balance equations at each time step, in order to update the evapotranspiration measure ET, as well as the other parameters needed to compute the crop's mass at the following time step.
The domain Ω of our choice is a cube of 1 meter side length, which represents the upper part of the cell, where air flows above the lettuce crops. In particular, the inlet is one whole face, the outlet is the whole opposite face, and the other lateral faces are walls. The top face is fully covered by LED lights, which provide violet illumination (and so heat) to the system. The bottom face is the interface with the crop leaves.
In this section, we consider the air as an incompressible, steady-state, Newtonian fluid and the flow is assumed to be laminar.
The coupled system is defined as:

$$\begin{cases} \operatorname{div}(\rho_a \mathbf{u}) = 0, & \text{in } \Omega \\ -\operatorname{div}[\mu(\nabla \mathbf{u} + \nabla \mathbf{u}^T)] + (\rho_a \mathbf{u} \cdot \nabla)\mathbf{u} + \nabla p = \mathbf{0}, & \text{in } \Omega \\ +\text{BCs} \end{cases} \tag{1}$$

where $\mathbf{u}$ $[ms^{-1}]$, the air fluid velocity, and p $[Pa]$, the pressure field, are the unknowns.
Moreover, ρ_a $[kgm^{-2}]$ and μ $[kgm^1s^{-1}]$ are respectively the air density and the dynamic viscosity.
Since we have assumed that air is an incompressible flow, we consider ρ_a constant. Moreover, μ does not change over the domain, and, defining $\nu = \frac{\mu}{\rho_a}$ as the kinematic viscosity, the system becomes:

$$\begin{cases} \operatorname{div}(\mathbf{u}) = 0, & \text{in } \Omega \\ -\nu\Delta\mathbf{u} + (\mathbf{u} \cdot \nabla)\mathbf{u} + \dfrac{1}{\rho_a}\nabla p = \mathbf{0}, & \text{in } \Omega \\ +\text{BCs} \end{cases} \tag{2}$$

where in the second equation the vanishing term has been removed.
System (2) allows us to compute the fluid velocity field of air ($\mathbf{u}$). This value is necessary to solve the energy balance equation:

$$\begin{cases} -\operatorname{div}(\lambda \nabla T_a) + \operatorname{div}(\rho_a C_p \mathbf{u} T_a) = 0, & \text{in } \Omega \\ +\text{BCs.} \end{cases} \tag{3}$$

C_p $[Jkg^{-1}K^{-1}]$ represents the specific heat capacity of air, while λ $[Wm^{-1}K^{-1}]$ the thermal conductivity: both are given constant values. We can simplify the equation in the following way, exploiting $\operatorname{div}(\mathbf{u}) = 0$.

$$\begin{cases} -\mu_T \Delta T_a + \mathbf{u} \cdot \nabla T_a = 0, & \text{in } \Omega \\ +\text{BCs} \end{cases} \tag{4}$$

where we have defined $\mu_T = \frac{\lambda}{\rho_a C_p}$.
Equation (4) provides us the unknown air temperature T_a $[K]$ as a scalar field in space within the cell, which computation was our primary aim in this section.
Physically speaking, within the cell there is a heat source, i.e. the LEDs that provide light to the system, and a sink, due to crop transpiration. However, both these phenomena are modelled through boundary conditions at top and bottom faces, as it will be illustrated in the apposite section (2.1.3). Indeed, the LEDs are located on the upper surface of the cell, while the lettuce is assumed to be right below the bottom face.
To make this simplification possible, we adopt the *Big-Leaf* approximation: the crops are modelled as one large leaf that occupies the whole base surface. The nature of this assumption will be discussed more in detail in the apposite section 2.3.1. In fact, we are assuming that the lettuce covers uniformly the whole bottom face, making easier to impose boundary conditions over this face.
Moreover, to keep our model computationally as light as possible, we assume that the crop grows only in weight and we neglect the growth in volume. This way we can consider the height of the domain for the air flow fixed in time.

2.1.2 Species Mass Fraction equations

We incorporate from [1] a conservation equation of the mass fraction, which applies to each of the species that make up the fluid. In particular, air is assumed here to be a mix of water vapor (H_2O), carbon dioxide (CO_2), oxygen (O_2), and nitrogen (N_2).
We indicate with γ_n the mass fraction of interest, where "n" could be any of the species listed above. $\mathbf{j}_n$ $[kgm^{-2}s^{-1}]$ represents the turbulent mass diffusion flux, R_n the rate of chemical production and S_n is a source term.

$$\begin{cases} \text{div}(\rho_a \mathbf{u} \gamma_n) = -\nabla \cdot \mathbf{j}_n + R_n + S_n, & \text{in } \Omega \\ \quad +\text{BCs.} \end{cases} \tag{5}$$

In our model, we are specifically interested in γ for H_2O and CO_2. These values will be indeed needed when performing an energy balance for the lettuce: γ_{H_2O} is used in (25), while γ_{CO_2} is involved in (18).
The mass diffusion flux $\mathbf{j}_n$ is described by the introduction of an appropriate Fick's law:

$$\mathbf{j}_n = -\rho_a D_n \nabla \gamma_n.$$

Here, the values for diffusion coefficients D_n $[m^2/s]$ are assumed constant and uniform and are taken from [4]. In particular, for the species of our interest we use:

- $D_{H_2O} = 2.178 \cdot 10^{-5}$
- $D_{CO_2} = 1.381 \cdot 10^{-5}$

The source term on the right-hand-side is set to zero. Indeed, the exchange of mass with the crop due to photosynthesis is taken into account through boundary conditions, as we will illustrate in section 2.1.3. Moreover, chemical reactions among different species are neglected.
Overall, the species mass fraction balance equation (5) can be written down as:

$$\begin{cases} -D_n \Delta \gamma_n + \mathbf{u} \cdot \nabla \gamma_n = 0, & \text{in } \Omega \\ \quad +\text{BCs} \end{cases} \tag{6}$$

where we have developed the gradient term $\text{div}(\rho_a \mathbf{u} \gamma_n)$, knowing that $\text{div}(\mathbf{u}) = 0$ from (2).

Remark 1. *Both the energy balance (4) and the species mass fraction balances (6) are advection-diffusion equations. This means that they can be written down in the general form $Lu = f$, where:*

$$L = -div(\mu \nabla) + \boldsymbol{b} \cdot \nabla \tag{7}$$

is the diffusion-advection operator and u is the generic unknown quantity to compute. μ the generic diffusion coefficient and $\boldsymbol{b}$ the generic advection coefficient.
The operator L can be split into the sum of a symmetric part L_S and a skew-symmetric part L_{SS},

$$Lu = L_S u + L_{SS} u. \tag{8}$$

In the case of study,

$$\begin{aligned} L_S u &= -div(\mu \nabla u) \\ L_{SS} u &= \boldsymbol{b} \cdot \nabla u \end{aligned} \tag{9}$$

2.1.3 Boundary Conditions

It has been already introduced the domain Ω of our choice. To improve clarity in this section, let us call I the inlet face, O the outlet face, B the bottom face (where there is the crop) and T the top face (where LED lights are positioned).
Mass and momentum balance equations (2) do not involve the presence of the crop. Hence, we impose no-slip condition on the four walls ($\partial\Omega/\{I, O\}$). Over the inlet face I we impose Dirichlet boundary condition, as the user is able to select whatever air flow velocity U through a fan. In the end, for the outlet face O, we opt for homogeneous Neumann condition.

$$\begin{cases} \text{div}(\mathbf{u}) = 0, & \text{in } \Omega \\ -\nu\Delta\mathbf{u} + (\mathbf{u}\cdot\nabla)\mathbf{u} + \nabla p = \mathbf{0}, & \text{in } \Omega \\ \mathbf{u} = \text{U}, & \text{on I} \\ \nu\nabla\mathbf{u}\cdot\mathbf{n} - p\cdot\mathbf{n} = 0, & \text{on O} \\ \mathbf{u} = 0, & \text{on } \partial\Omega/\{I, O\} \end{cases} \tag{10}$$

As regards the energy balance (3), we impose Dirichlet boundary conditions at the inlet face, fixing the temperature to the one of the outside environment, that is $T_{amb} = 25°\text{C}$. On the outlet face homogeneous Neumann condition is imposed. On the top face, we set Neumann boundary conditions to represent heat flux provided by the lights to the system.
Through the bottom face, heat is transferred to the lettuce in order to allow the crop transpiration process. This is modelled again through a Neumann boundary condition at face B.
In the end, on the remaining lateral faces we impose homogeneous Neumann boundary conditions, as there is no heat flux through walls.

$$\begin{cases} -\mu_T \Delta T_a + \mathbf{u}\cdot\nabla T_a = 0, & \text{in } \Omega \\ T_a = T_{amb}, & \text{on I} \\ \nabla T_a \cdot \mathbf{n} = -\dfrac{I_{light}}{\lambda}, & \text{on T} \\ \nabla T_a \cdot \mathbf{n} = Q_l, & \text{on B} \\ \nabla T_a \cdot \mathbf{n} = 0, & \text{on } \partial\Omega/\{I, T, B\} \end{cases} \tag{11}$$

Q_l is the amount latent heat that is absorbed by the lettuce at a certain time. We have already explained how this value is the actual sought output of our whole model (ET can be easily and directly computed after Q_l, as it will be explained in section 2.3.3). Therefore, the value considered in (11) is the one computed at the previous time iteration, resulting as a feedback.
At the first iteration, we simply put $Q_l = 0$. This is reasonable enough as the lettuce, even if it has already (very small) mass and volume, is newly planted. The led lights intensity I_{light} $[W/m^2]$ of the top wall corresponds naturally to the heat flux imposed at that boundary. *Agricola Moderna* suggested us to set $I_{light} = 45\ W/m^2$.

To conclude this section, we consider the species mass fraction equations.
Air flow comes from the inlet and exits from the outlet, hence the same happens to air particles of each species. To model this, we set Dirichlet boundary conditions on the inlet face, where we

impose continuity with the concentrations $\gamma_{amb,n}$ outside the cell. On the other hand, we set homogeneous Neumann conditions at the outlet face. Over the bottom surface B, we set a non-homogeneous Neumann boundary condition to model the mass of CO_2 and H_2O that is absorbed by the crop to photosynthesize. Moreover, it is physically impossible for the particles to pass through the walls. It follows quite naturally the imposition of homogeneous Neumann boundary conditions also at the four lateral wall faces.
Overall, equation (6) with appropriate boundary conditions becomes:

$$\begin{cases} -D_n\Delta\gamma_n + \mathbf{u}\cdot\nabla\gamma_n = 0, & \text{in } \Omega \\ \gamma_n = \gamma_{amb,n}, & \text{on } I \\ \nabla\gamma_n\cdot\mathbf{n} = S_n, & \text{on } B \\ \nabla\gamma_n\cdot\mathbf{n} = 0, & \text{on } \partial\Omega/\{I,B\} \end{cases} \tag{12}$$

In [3] the carbon dioxide mass fraction and the relative humidity at inlet are specified. We adopt the same values:

$$\gamma_{amb,CO_2} = 0.00153,$$
$$\gamma_{amb,H_2O} = 0.85$$

The flux term S_n represents the mass flow rate of both CO_2 and H_2O that are absorbed by the crop. At the first iteration we simply put $S_n = 0$ for both carbon dioxide and water, as we assume the crop is too small when newly planted to perform a photosynthesis which requires non-negligible amount of reagents. After that, at each iteration the computation of S_n is discussed in detail in section 2.2.3.

Remark 2. *In the previous remark 1, it was already highlighted how both 11 and 12 are advection-diffusion equations, both having the same transport velocity (the fluid velocity* $\mathbf{u}$*). It comes quite naturally that also the boundary conditions are almost the same. In both cases the lettuce represents a sink. The only difference is at the top boundary: the LEDs provide heat to the system, but clearly they do not provide mass.*
In both equations, at initial time the sink effect of the newly planted crop is physically negligible: it is translated in homogeneous Neumann conditions. By advancing in time, sink grows with the crop weight. In results section 5.3 it is possible to visualize the difference between the initial and the final time.

2.2 Dry weight model

In this section we focus on the development of an equation that provides the evolution in time of the dry weight DW $[g]$ of the crop as a function of the cell climate.
The main idea here is to divide the dry weight into two components, as it is done in [2]: the *structural* dry weight (X_{sdw}) and the *non structural* dry weight (X_{nsdw}), which consists of glucose, sucrose, starch, etc..
Despite what we did in the previous section, here we are interested only in the time dependence of the variables, as we refer to *overall* dry weight. For this reason we develop a lumped model, hence the system is considered to be zero-dimensional, i.e. a single point. In this way we are ignoring spatial gradients: only the time dependence of the different variables we are about to introduce has relevance. Both X_{sdw}, X_{nsdw} are dimensionally $[gm^{-2}]$, so we just obtain the total dry weight as the sum of the two contributions.

$$DW(t) = X_{sdw}(t) + X_{nsdw}(t)$$

The dynamic behavior of the dry weight is indeed presented in [2], resulting in the following system of ODEs.

$$\begin{cases} \dfrac{d}{dt}X_{nsdw}(t) = c_\alpha f_{phot}(t) - r_{gr}(t)X_{sdw}(t) - f_{resp}(t) - \dfrac{1-c_\beta}{c_\beta}r_{gr}(t)X_{sdw}(t) \\ \dfrac{d}{dt}X_{sdw}(t) = r_{gr}(t)X_{sdw}(t) \end{cases} \tag{13}$$

The coefficients are known:

- $c_\alpha = 30/44 \approx 0.68$ is the ratio of molecular weight of CH_2O (sugar) and CO_2;
- $c_\beta = 0.8$ indicates the respiratory and synthesis losses of non-structural material due to growth.

Moreover, the model involves other evolution variables that need to be computed:

- f_{phot} $[gm^{-2}s^{-1}]$ is the gross canopy photosynthesis;
- f_{resp} $[gm^{-2}s^{-1}]$ is the maintenance respiration;
- r_{gr} $[s^{-1}]$ is a specific growth rate that describes the transformation rate of non-structural dry weight into structural dry weight.

In order to close the system, we need an equation for each of these variables. These further needed relations are discussed in the subsection 2.2.2.
It is crucial to remark that the parameter f_{phot} plays an essential role in our model. Indeed, not only it is needed to compute the dry weight as shown in (13), but also it appears in the definition of the boundary conditions in (6). The subsection 2.2.3 is dedicated to a deeper explanation of the role of f_{phot} in the mass fraction balance.

2.2.1 Climate variables

Before proceeding with showing the remaining equations needed to close the system, we remark that we are developing a model for the crop evolution in time, knowing the climatic conditions of the cell from the previous treatment. In particular, the model (13) uses as input variables the air temperature T_a and the carbon dioxide concentration γ_{CO_2}. We have already computed these variables as scalar fields in (3) and (6) respectively.
In this section we are considering the system as lumped: we are interested only in the evolution in time of the lettuce dry weight, without considering spatial gradients. To *extrapolate* a uniform, averaged scalar variable for the CO_2 concentration, we compute the integral mean over the fluid domain, which has unitary volume. Hence, we approximate:

$$\gamma_{CO_2} \approx \int_\Omega \gamma_{CO_2}(\mathbf{x}) d\Omega \tag{14}$$

Similarly we approximate the value for the air temperature T_a.

$$T_a \approx \int_\Omega T_a(\mathbf{x}) d\Omega \tag{15}$$

To estimate the canopy temperature T_c, we were suggested directly by *Agricola Moderna* to assume that the lettuce is always 1 degree colder than air.

$$T_c \approx T_a - 1$$

This might seem a rough approximation, but looking at experimental data it is actually reasonable enough for our aims.

2.2.2 Further needed relations

In order to close system (13), we need three independent equations for the functions f_{phot}, f_{resp}, r_{gr}. Again, such relations are provided by [2] and are presented in the system below.

$$\begin{cases} f_{phot}(t) = (1 - exp(-c_K c_{lar}(1-c_\tau)X_{sdw}(t)))f_{phot,max} \\ f_{resp}(t) = (c_{resp,sht}(1-c_\tau)X_{sdw}(t) + c_{resp,rt}c_\tau X_{sdw}(t))c_{Q_{10,resp}}^{\frac{T_c-25}{10}} \\ r_{gr}(t) = c_{gr,max}\dfrac{X_{nsdw}(t)}{X_{sdw}(t)+X_{nsdw}(t)}c_{Q_{10,gr}}^{\frac{T_c-20}{10}} \end{cases} \tag{16}$$

where the several coefficients are either found in literature or estimated by experimental data ([2]).
More in details, the transformation of non-structural into structural material is proportional to the fraction of dry weight which is non-structural; also it depends on the temperature. In particular, the dependence on temperature of r_{gr} relies on the Q_{10} [1] factor for growth: $c_{Q_{10},gr} = 1.6$. $c_{gr_max} \approx 5 \times 10^{-6}\ s^{-1}$ is the saturation growth rate.
The maintenance respiration rate of the crop f_{resp} is expressed in terms of two distinct contributions related to the shoot and the root. They have a different maintenance respiration coefficient:

$$c_{resp,rt} \approx 1.16 \times 10^{-7} s^{-1},$$
$$c_{resp,rt} \approx 1.16 \times 10^{-7} s^{-1}$$

These two terms are weighted by the parameter $c_{tau} = 0.15$, which is indeed the ratio of the root dry weight and the total dry weight, and it is assumed to remain constant as the crop grows. As for the transformation rate, the temperature dependence of maintenance respiration process relies on an apposite Q_{10} factor: $c_{Q_{10},resp} = 2$.
Last, the gross canopy photosynthesis f_{phot} is bounded by its theoretical maximum value, $f_{phot,max}$, which is defined as the gross carbon dioxide assimilation rate of the canopy at complete soil covering, and a coefficient that takes into account the geometrical and optical properties of the canopy when the soil is not completely covered, hence when the incident radiation is not fully absorbed.
Remark that, even if we did the *Big-Leaf* assumption in section 2.1.1, in this equation we still consider a more realistic scenario where the lettuce does not cover the whole surface of the soil. We do this because f_{phot} is of crucial importance in our model: it will be explained in section 2.2.3 how it works as a feedback agent. For this reason, we consider convenient to adopt the full equation for f_{phot} provided by [2]. Another reason is that the coefficient of $f_{phot,max}$ does not complicate too much our model and introduces the dependence of the photosynthesis on the dry weight.
The coefficients are: the extinction coefficient $c_K \approx 0.9$ and the structural leaf area $c_{lar} \approx 75 \times 10^{-3}$ $m^2 g^{-1}$.
The gross carbon dioxide assimilation rate $f_{phot,max}$ $[gm^{-2}s^{-1}]$ is described by a rectangular hyperbola, that involves the dependence on incident radiation I_{light} (introduced in section 2.1.3) and on carbon dioxide concentration γ_{CO_2} (computed previously in section 2.2.1).

$$f_{phot,max} = \frac{\varepsilon I_{light} g_{CO_2} c_\omega (\gamma_{CO_2} - \Gamma)}{\varepsilon I_{light} + g_{CO_2} c_\omega (\gamma_{CO_2} - \Gamma)} \tag{17}$$

Where ϵ $[gJ^{-1}]$ is the light use efficiency, Γ $[ppm]$ is the CO_2 compensation point, accounting for photo-respiration at high light levels and g_{CO_2} $[ms^{-1}]$ is the canopy conductance to CO_2 diffusion. $c_\omega \approx 1.83 \times 10^{-3}\ gm^{-3}$ is the estimated CO_2 density at 15° temperature and ambient pressure.
For each of these parameters, [2] provides an expression that allows us to compute them:

$$\begin{cases} \Gamma = c_\Gamma c_{Q_{10},\Gamma}^{\frac{T_c - 20}{10}} \\ \epsilon = c_\epsilon \dfrac{\gamma_{CO_2} - \Gamma}{\gamma_{CO_2} + 2\Gamma} \\ \dfrac{1}{g_{CO_2}} = \dfrac{1}{g_{bnd}} + \dfrac{1}{g_{stm}} + \dfrac{1}{g_{car}} \\ g_{car} = c_{car,1} T_c^2 + c_{car,2} T_c + c_{car,3} \end{cases} \tag{18}$$

In particular:

- $c_\Gamma = 40\ ppm$ is the value of Γ at 20°;
- $c_{Q_{10},\Gamma} = 2$ is the temperature coefficient for the CO_2 compensation point;
- $c_\epsilon = 17.0 \times 10^{-6}\ gJ^{-1}$ is the value of ϵ at very high CO_2 concentrations;

[1] The Q_{10} factor, also known in literature as temperature coefficient, is a non-dimensional quantity that measures temperature sensitivity of chemical reaction rates or biological processes ([5])

- g_{bnd} $[ms^{-1}]$ is the boundary layer conductance;
- g_{stm} $[ms^{-1}]$ is the stomatal conductance;
- g_{car} $[ms^{-1}]$ is the carboxylation conductance, with $c_{car,1} = -1.32 \times 10^{-5}$ $[ms^{-1\circ}C^{-2}]$, $c_{car,2} = 5.94 \times 10^{-4}$ $[ms^{-1\circ}C^{-2}]$ and $c_{car,3} = -2.64 \times 10^{-3}$ $[ms^{-1\circ}C^{-2}]$;

At this point, our model for the dry weight is closed.
In particular, it is relevant for us the structural dry weight X_{sdw}, as it allows us to compute the leaf area index, that will be introduced in section 2.2.4.
Also, we had the chance to introduce a measure for the photosynthesis f_{phot}, that has a pivotal role in our model overall. Not only it acts as a feedback variable, but also involves itself the leaf area index, as we will show next.

2.2.3 Feedback action with photosynthesis

As we wrote right above, a relevant output of the system (13) is indeed the gross canopy photosynthesis f_{phot}, which provides us the amount of CO_2 mass that is consumed by the crop's photosynthesis. Indeed, this value must be included in the species mass fraction balance (6) for the carbon dioxide. In this way, we are introducing here a feedback in our model.
In particular, f_{phot} $[g/m^2s]$ is directly used to determine the mass flux from the environment toward the canopy for the carbon dioxide S_{CO_2} $[kg/m^2s]$, after a suitable change in the unit of measure[2]

$$S_{CO_2} = -f_{phot} \times 10^{-3} \quad kgm^{-2}s^{-1} \tag{19}$$

On the other hand, the H_2O consumption rate S_{H_2O} is calculated and set based on the molar balance of the photosynthesis reaction equation:

$$6CO_2 + 6H_2O \rightarrow C_6H_{12}O_6 + 6O_2. \tag{20}$$

According to the reaction, 6 moles of CO_2 react with 6 moles of H_2O ($n_{CO_2} = n_{H_2O} = 6$). The molar mass of CO_2 and H_2O are 44.01 g/mol and 18.02 g/mol respectively, and we know that the amount of mass is given by

$$m_{H_2O} = n_{H_2O} \times 18.02\ g/mol, \qquad m_{CO_2} = n_{CO_2} \times 44.01\ g/mol.$$

Therefore, we can easily calculate the H_2O consumption rate to use in (6) from f_{phot}:

$$S_{H_2O} = \left(\frac{18.02}{44.01}\right) \times S_{CO_2}\ kgm^{-2}s^{-1} \tag{21}$$

2.2.4 Leaf Area Index

The Leaf Area Index, LAI, is a non-dimensional biophysical quantity that is widely used in soil-plant relationship. It has application in models (like this one) for crop growth, photosynthesis and transpiration. In literature, it is possible to find several definitions for this quantity; briefly, it expresses the leaf area per unit ground.
Actually, the computation of the LAI, together with the definition of the species mass fraction fluxes through f_{phot}, is the ultimate aim of the model for the dry weight presented in this section. Indeed, the knowledge of the LAI is necessary to perform an energy balance for the crop, as we will show in the following section 2.3.
In literature, there is a wide variety of methods and formulas to measure in the most accurate way the leaf area index. In our model we rely on the relation provided by [2], in order to stay coherent with the computation of f_{phot}.

$$LAI = (1 - c_\tau) c_{lar} X_{sdw}(t) \tag{22}$$

It is indeed possible to notice that LAI was "hidden" inside the equation for f_{phot}.
Now that we have computed the leaf area index, we are able to perform a crop energy balance that would allow us to, finally, compute the latent heat and to measure evapotranspiration.

[2] We divide by 10^3 to convert grams in kilograms.

2.3 Crop energy balance

To complete our model for evapotranspiration, we need to perform an energy balance of the crop. This section was adapted from [3], where it is done a study of the crop transpiration in plant factories. Again, as it was for the Navier-Stokes system of equations discussed in section 2.1, we are considering steady-state variables. In fact, as it will be explained in section 3 concerning the numerical discretization, we perform a crop energy balance at each time step, with updated values of dry weight, temperature, photosynthesis, species concentrations, leaf area index etc.

2.3.1 Big-Leaf approximation

At the base of this treatment there is an important assumption, that is the adoption of the so called Big-Leaf model: the three dimensional crop canopy is reduced to a one *big leaf* where net radiation is absorbed, heat is exchanged and water vapour escapes due to evapotranspiration.
This assumption was already introduced in section 2.1, where we assumed the crop to have fixed height and to cover uniformly the bottom boundary face. We are allowed to make this assumption since in the cell the crop is assumed to be homogeneous, level, continuous and extensive enough. For simplicity, this is assumed to be true not only when the lettuce is ready to be harvested, but at every time, without implementing a "volumetric" growth of the canopy.
This assumption allows us to have a cubic, regular shape for the fluid domain. This keeps the air flow laminar, leading us to simplify a lot our mathematical model, as well as the computational cost of its implementation.
The idea is taken from a popular model for evapotranspiration measurement: the Penman-Monteith equation. This model is considered one of the most reliable ones in terms of accuracy for practical purposes, and it is included in the FAO guidelines for the calculation of reference and crop evapotranspiration ([6]). Therefore, albeit the big-leaf might look like as a very rough approximation from the physical point of view, it is actually not that bad in terms of results. The discussion done in [3] relies on the Penman-Monteith model, and so do we.

2.3.2 Model for latent heat of evaporation

The impact of the crop in the surrounding environment is very relevant, in fact it exchanges heat, absorbs/emit radiation and it transpires. In particular, the latter is the process of our main interest. Thanks to the *big leaf* approximation, we can consider the lettuce as a uniform body. As a consequence, we can treat the crop as a zero-dimensional system, hence we can ignore spatial gradients and assume all the canopy properties to be uniform.
At equilibrium, the overall energy arriving at the *big leaf* equals the amount leaving it:

$$R_{net} - Q_h - Q_l = 0 \tag{23}$$

Where:

- R_{net} $[Wm^{-2}]$ is the net radiation *absorbed* by the crop;
- Q_h $[Wm^{-2}]$ is the sensible heat flux;
- Q_l $[Wm^{-2}]$ is the latent heat flux.

One could easily imagine that R_{net} is proportional to the light intensity set for the LEDs (I_{light}). The proportionality constant is made by some reflection coefficient $\rho_r \approx 0.05 - 0.08$ and by another parameter $CAC \approx 0.9$. The latter is the ratio of projected leaf area to cultivation area, which is considered almost constant in lettuce throughout its development. In fact, CAC is a sort of correction term that is needed under the *big leaf* approximation.

$$R_{net} = (1 - \rho_r) I_{light} CAC \tag{24}$$

Therefore R_{net} only depends on the light intensity, which can be set by the user. This means that this term is basically a control variable itself. As a consequence, in (23), R_{net} is known and constant in time. On the other hand, for the heat fluxes, we rely on the following relations:

$$\begin{cases} Q_h = LAI\rho_a C_p \dfrac{T_c - T_a}{r_a} \\ Q_l = LAI\lambda_v \dfrac{\gamma_{H_2O,c} - \gamma_{H_2O,a}}{r_s + r_a} \end{cases} \tag{25}$$

Both equations incorporate the leaf area index, which was computed in (22), in order to account for the effective transpiring surface instead of the total leaf area.
The sensible heat flux Q_h is proportional to the air mass density ρ_a and to the specific heat capacity of air C_p. Since the air flow was assumed to be incompressible, both these values are known coefficients, already introduced in (1) and (3). Moreover, we introduced in section 2.2.1 the assumption that the canopy is always 1°C colder than air, thereby $T_c - T_a = -1$ at whatever time, so Q_h has always a negative value. Within the energy balance, Q_h is considered as heat exchanged from the crop to the air. This is coherent with the introduced notation and respects the second law of thermodynamics: the crop's surface is colder than the air, so the crop absorbs heat form the environment. The sensible heat flux encounters a single kind of resistance: the aerodynamics resistance to heat r_a $[sm^{-1}]$.
The latent heat flux Q_l is defined as λ_v $[Jg^{-1}]$, the latent heat of evaporation of water, scaled with LAI and the difference in H_2O concentration between the crop and the air. Moreover, the vapour flux from the crop to air encounters two kinds of resistances: r_a and r_s $[sm^{-1}]$, which is the stomatal resistance of vapour flow through the transpiring crop. We observe that Q_l must be positive, as the sum $R_{net} - Q_h$ is for sure positive after the discussion done above. This makes sense as the latent heat Q_l is absorbed by the crop in order to transpire: the liquid water contained in the canopy evaporates and it is expelled through the stomata as water vapour.
In (6) we computed the H_2O mass fraction in the air flow domain as a scalar field. Here, as we are neglecting spatial gradients, we compute one value for water concentration in air $\gamma_{H_2O,a}$ by performing an integral mean.[3]

$$\gamma_{H_2O,a} \approx \int_\Omega \rho_a \gamma_{H_2O}(\mathbf{x}) d\Omega$$

In fact, we are using the same logic we already introduced in section 2.2.1 to compute a single value for T_a and γ_{CO_2}.
To estimate the air concentration in the crop, we perform another integral mean, but this time just over the bottom face, which is the interface between air and lettuce.

$$\gamma_{H_2O,c} \approx \int_B \rho_a \gamma_{H_2O}(\mathbf{x}) dB$$

Here $\gamma_{H_2O,i}$ for $i = a, c$ are needed in $[g/m^3]$, so we include in the averaging procedure also the air mass density ρ_a.
To conclude, we close the system by writing down a definition for the two resistances introduced above. r_a represents the resistance to heat and vapour transfer due to the aerodynamic boundary layer. The fact that it has to do with turbulence in the boundary layer explains the dependence on $l = 0.11$, the mean leaf diameter, that works as a sort of characteristic length for a leaf and u_∞ the uninhibited air speed. We take u_∞ equal to the Dirichlet boundary condition value for the y-direction velocity at the inlet in equation (10).
On the other hand, the stomatal resistance, r_s, is known and it depends on the photosynthetic photon flux density $PPFD$ $[\mu molm^{-2}s^{-1}]$. The light intensity can be very easily converted into $PPFM$:

$$PPFM = 4.6 \times I_{light} \quad \mu molm^{-2}s^{-1}$$

The conversion value "4.6" has been provided by *Agricola Moderna* and it is related with the light spectrum of the emitted radiation. Hence, once the user sets its preferred light intensity for the LEDs on the top wall, the stomatal resistance is automatically known without involving other dependences.

[3] Fluid domain Ω has unitary volume

$$\begin{cases} r_s = 60\dfrac{1500 + PPFD}{200 + PPFD} \\ r_a = 350(\dfrac{l}{u_\infty})^{0.5} LAI^{-1} \end{cases} \tag{26}$$

As r_a concerns the boundary layer, it is clear that it increases a lot with turbulence. Albeit in our model we are assuming to be in a controlled environment (such as a unit cell of a vertical farm) and to have laminar flow, we include anyway the (small) contribution of this resistance. Indeed, the equation we use is suited for controlled environment with relatively high circulation rate. The relation for r_s is instead built up starting from experimental data.
We have concluded our detailed discussion about the crop energy balance and its players. At this point, having previously done all the computations presented in sections 2.1 and 2.2, our unknowns are the latent heat Q_l and the latent heat of evaporation λ_v, which happen indeed to be the variables of our interest. So we solve the system

$$\begin{cases} Q_l = R_{net} - Q_h \\ Q_l = LAI\lambda_v \frac{\gamma_{H_2O,c} - \gamma_{H_2O,a}}{r_s + r_a} \end{cases} \tag{27}$$

obtaining, in the end, the following relation for the latent heat of water evaporation:

$$\lambda_v = (R_{net} - Q_h)\frac{r_s + r_a}{LAI(\gamma_{H_2O,c} - \gamma_{H_2O,a})} \tag{28}$$

2.3.3 Evapotranspiration

Transpiration is a process that consists of the vaporization of liquid water contained in plant tissues and the vapour removal to the atmosphere. Crops predominantly lose their water through stomata: small openings on the plant leaf through which gases and water vapour pass. Moreover, water vapour is also released in the surrounding environment by evaporation of the liquid water contained in the soil surface. There is no easy way of distinguishing between the two processes of crop transpiration and evaporation from the soil, this is why they are usually combined and modelled as one process: evapotranspiration. Therefore, to sum up, evapotranspiration is the combination of two processes through which liquid water, contained in both the crop and the soil surface, evaporates, becoming water vapour released in the environment ([6]).
We pointed out in the first pages of this report that our final aim is to provide a measure of evapotranspiration in our cell configuration. In particular we define ET $[gm^{-2}s^{-1}]$ as the rate of water vapour mass released.
Having computed in section 2.3.2 the value of the latent heat Q_l $[W/m^2]$ and the latent heat of evaporation λ_v it turns out to be very easy the computation of such evapotranspiration mass rate:

$$ET = \frac{Q_l}{\lambda_v} = LAI\frac{(\gamma_{H_2O,c} - \gamma_{H_2O,a})}{(r_s + r_a)} \tag{29}$$

3 Numerical Discretization

After presenting the entire mathematical model in the previous chapter, here we focus on its numerical discretization in time and in space.
As discussed in Section 2, time evolution is only considered in the dry weight equations. Therefore, to compute (13), we only need a time discretization Δt and, as explained in section 4.3, which is dedict to solve the system we will employ the Crank-Nicolson method.
On the other hand, the system of PDEs concerning the flow rate, the temperature and the species mass fraction requires some further analysis. Indeed, in order to be simulated by the software, those steady-state PDEs need to be discretized in space. In particular, the software used in our case is `FreeFem++`, that is based on Finite Element method (FEM).
Here, we first derive the weak formulation of the PDEs, subsequently we obtain their finite element formulation.

3.1 Navier - Stokes equations

We start analyzing the Navier-Stokes equations (2). The first step consists in the deduction of the dimensionless equations. At this scope, we introduce the Reynolds number (Re), an adimensional quantity that measures the ratio between inertial and viscous forces, defined as

$$Re = \frac{\rho_a U L}{\mu}, \tag{30}$$

where U and L are respectively the characteristic velocity and characteristic length of the system. We took as L the side length of the cubic domain, while U is the inlet air velocity introduced in section 2.1.3. The evaluation of Re gives us also a confirm of the assumption of laminar flow. The adimensional form of the Navier–Stokes equations is introduced to simplify the analysis of the problem and reduce the number of free parameters. Moreover, dimensionless equations help to gain a greater insight into the relative size of various terms present in them. The resulting adimensional system ([7]) is:

$$\begin{cases} \operatorname{div}(\mathbf{u}) = 0, & \text{in } \Omega \\ -\dfrac{1}{Re}\Delta\mathbf{u} + (\mathbf{u}\cdot\nabla)\mathbf{u} + \nabla p = \mathbf{0}, & \text{in } \Omega \\ +\text{BCs} \end{cases} \tag{31}$$

Remark 3. *We highlight that in the momentum equation we are considering and calling "pressure" the quantity p, which, in reality, is the so-called excess pressure,*

$$p_e = \frac{p - p_{static}}{\rho_a}$$

where p_{static} is the part of pressure balanced by gravity.

To obtain the weak formulation, we multiply the momentum equation by a test function $\mathbf{v}$ belonging to a suitable space $\mathbf{V}$, that will be specified later on. Then, we integrate over the entire domain Ω and, rearranging the terms, we obtain:

$$\int_\Omega \{(\mathbf{u}\cdot\nabla)\mathbf{u}\cdot\mathbf{v} + \nabla p\cdot\mathbf{v} - \frac{1}{Re}\Delta\mathbf{u}\cdot\mathbf{v}\} d\Omega = 0 \quad \forall \mathbf{v}\in\mathbf{V}. \tag{32}$$

Under the assumption we will specify below, we can employ the Green formula and integrate by part the following terms:

$$-\int_\Omega \frac{1}{Re}\Delta\mathbf{u}\cdot\mathbf{v}\, d\Omega = \int_\Omega \frac{1}{Re}\nabla\mathbf{u} : \nabla\mathbf{v}\, d\Omega - \int_{\partial\Omega}\frac{1}{Re}(\nabla\mathbf{u}\cdot\mathbf{n})\cdot\mathbf{v}\, d\Gamma \quad \forall\mathbf{v}\in\mathbf{V} \tag{33}$$

$$\int_\Omega \nabla p\cdot\mathbf{v}\, d\Omega = -\int_\Omega p\, \operatorname{div}(\mathbf{v})\, d\Omega + \int_{\partial\Omega} p\mathbf{v}\cdot\mathbf{n}\, d\Gamma \quad \forall\mathbf{v}\in\mathbf{V}. \tag{34}$$

Consequently, the momentum equation becomes:

$$\int_\Omega (\mathbf{u}\cdot\nabla)\mathbf{u}\cdot\mathbf{v} + \int_\Omega \frac{1}{Re}\nabla\mathbf{u}:\nabla\mathbf{v}\, d\Omega - \int_\Omega p\, \operatorname{div}(\mathbf{v})\, d\Omega - \int_{\partial\Omega}(\frac{1}{Re}\nabla\mathbf{u}\cdot\mathbf{n} - p\mathbf{n})\mathbf{v}\, d\Gamma = 0 \quad \forall\mathbf{v}\in\mathbf{V} \tag{35}$$

Similarly, in the continuity equation, we multiply by a test function q belonging to a suitable space Q, to be specified, then integrating on Ω it follows:

$$\int_\Omega q(\operatorname{div}(\mathbf{u}))\, d\Omega = 0 \quad \forall q\in Q \tag{36}$$

Customarily, $\mathbf{V}$ is chosen so that the test functions vanish on the boundary portion where a Dirichlet data is prescribed on $\mathbf{u}$, that is $\mathbf{V} = [H^1_{\Gamma_D}(\Omega)]^3 = \{\mathbf{v}\in[H^1(\Omega)]^3 : \mathbf{v}|_{\Gamma_D} = 0\}$. On the other hand, due to the non-emptiness of Γ_N, Q can be chosen as $Q = L^2$. Moreover, $\mathbf{u}\in[H^1(\Omega)]^3$, $p\in Q$. Consequently, in (35) the integral over $\partial\Omega$ vanishes in Γ_D and the equation simplifies in:

$$\int_\Omega (\mathbf{u}\cdot\nabla)\mathbf{u}\cdot\mathbf{v} + \int_\Omega \frac{1}{Re}\nabla\mathbf{u}:\nabla\mathbf{v}\, d\Omega - \int_\Omega p\, \operatorname{div}(\mathbf{v})\, d\Omega - \int_{\Gamma_N}(\frac{1}{Re}\nabla\mathbf{u}\cdot\mathbf{n} - p\mathbf{n})\mathbf{v}\, d\Gamma_N = 0 \quad \forall\mathbf{v}\in\mathbf{V} \tag{37}$$

Furthermore, we impose homogeneous Neumann boundary conditions: the integral over Γ_N vanishes and the obtained system is:

$$\begin{cases} \displaystyle\int_\Omega (\mathbf{u}\cdot\nabla)\mathbf{u}\cdot\mathbf{v} + \int_\Omega \frac{1}{Re}\nabla\mathbf{u} : \nabla\mathbf{v}\ d\Omega - \int_\Omega p\ \mathrm{div}(\mathbf{v})\ d\Omega = 0 \quad \forall \mathbf{v}\in\mathbf{V} \\ \displaystyle\int_\Omega (\mathrm{div}(\mathbf{u}))q\ d\Omega = 0 \quad \forall q \in Q \end{cases} \tag{38}$$

Under the considered assumption every term of the system is well defined, as the integrals are all finite. Indeed, it can be proved that:

$$\begin{aligned} &\left|\int_\Omega \nabla\mathbf{u} : \nabla\mathbf{v} d\Omega\right| \le |\mathbf{u}|_{[\mathbf{H}^1(\Omega)]^3}|\mathbf{v}|_{[\mathbf{H}^1(\Omega)]^3} \\ &\left|\int_\Omega p(\mathrm{div}(\mathbf{v}))d\Omega\right| \le ||p||_{L^2(\Omega)}|\mathbf{v}|_{[\mathbf{H}^1(\Omega)]^3} \\ &\left|\int_\Omega q(\mathrm{div}(\mathbf{u}))d\Omega\right| \le ||q||_{L^2(\Omega)}|\mathbf{u}|_{[\mathbf{H}^1(\Omega)]^3} \\ &\left|\int_\Omega (\mathbf{u}\cdot\nabla)\mathbf{u}\cdot\mathbf{v} d\Omega\right| \le ||\nabla\mathbf{u}||_{L^2(\Omega)}||\mathbf{u}||_{L^4(\Omega)}||\mathbf{v}||_{L^4(\Omega)} \le C^2||\mathbf{u}||^2_{[\mathbf{H}^1(\Omega)]^3}||\mathbf{v}||_{[\mathbf{H}^1(\Omega)]^3} \end{aligned}$$

where, for every function $\mathbf{v}\in[\mathbf{H}^1(\Omega)]^3$ we denote the norm by

$$||\mathbf{v}||_{[\mathbf{H}^1(\Omega)]^3} = \left(\sum_{k=1}^3 ||v_k||^2_{H^1(\Omega)}\right)^{1/2}$$

and the seminorm by

$$|\mathbf{v}|_{[\mathbf{H}^1(\Omega)]^3} = \left(\sum_{k=1}^3 |v_k|^2_{H^1(\Omega)}\right)^{1/2}.$$

We then introduce:

- a bilinear form $a(\cdot,\mathbf{z},\mathbf{w},\cdot) : \mathbf{V}\times\mathbf{V}\to\mathbb{R}$ as[4]:

$$a(\mathbf{u},\mathbf{z},\mathbf{w},\mathbf{v}) = \int_\Omega \frac{1}{Re}\nabla\mathbf{u} : \nabla\mathbf{v} + ((\mathbf{z}\cdot\nabla)\mathbf{u} + (\mathbf{u}\cdot\nabla)\mathbf{w})\cdot\mathbf{v}\ d\Omega \quad \text{for all } \mathbf{u},\mathbf{v}\in\mathbf{V}$$

- a bilinear form $b(\cdot,\cdot) : \mathbf{V}\times Q\to\mathbb{R}$ such that:

$$b(\mathbf{v},q) = -\int_\Omega q(\mathrm{div}\mathbf{v})d\Omega \quad \text{for all } \mathbf{v}\in\mathbf{V}, q\in Q$$

The obtained formulation of the problem is:

$$\begin{cases} a(\mathbf{u},\mathbf{u},\mathbf{0},\mathbf{v}) + b(p,\mathbf{v}) = 0 & \text{for all } \mathbf{v}\in\mathbf{V}, \\ -b(\mathbf{u},q) = 0 & \text{for all } q\in Q \end{cases} \tag{39}$$

Since the Dirichlet boundary condition for our problem are $\mathbf{u} = U$ on I and $\mathbf{u} = 0$ on $\{\Gamma_D\backslash I\}$, we introduce a continuous lifting operator $\mathbf{R}_I$ such that $\mathbf{R}_I\in\mathbf{H}^1(\Omega)$ and $\mathbf{R}_I|_I = U$. We define a new unknown function $\dot{\mathbf{u}} = \mathbf{u} - \mathbf{R}_I$ that, by construction, belongs to $\mathbf{H}^1_{\Gamma_D}(\Omega)$. By replacing $\mathbf{u}$ in (39) with $\dot{\mathbf{u}} + \mathbf{R}_I$, we get:

$$\begin{cases} a(\dot{\mathbf{u}},\dot{\mathbf{u}},\mathbf{0},\mathbf{v}) + b(p,\mathbf{v}) = \tilde{F}(\mathbf{v}) & \text{for all } \mathbf{v}\in\mathbf{V}, \\ -b(\dot{\mathbf{u}},q) = G(q) & \text{for all } q\in Q \end{cases} \tag{40}$$

[4]Note that this bilinear form is slightly different from the one introduced during the course lectures, but it is useful for our numerical implementation, as explained in the Section 4

where $\tilde{F}(\mathbf{v}) = -a(\mathbf{R}_I, \mathbf{R}_I, \mathbf{0}, \mathbf{v})$ and $G(q) = -b(\mathbf{R}_I, q)$. From now on we write $\dot{\mathbf{u}} = \mathbf{u}$ to simplify the notation.
Finally, the weak formulation of Navier-Stokes equations (1) reads:
find $(\mathbf{u}, p) \in \mathbf{V} \times Q$ such that:

$$\begin{cases} a(\mathbf{u}, \mathbf{u}, \mathbf{0}, \mathbf{v}) + b(p, \mathbf{v}) = \tilde{F}(\mathbf{v}) & \text{for all } \mathbf{v} \in \mathbf{V}, \\ -b(\mathbf{u}, q) = G(q) & \text{for all } q \in Q \end{cases} \tag{41}$$

In order to be able to solve the problem with a Finite Element Method, we introduce a suitable triangulation of the domain $\boldsymbol{\tau}_h$ (we will study the size of this mesh in the next section). Then, we consider two families of finite-dimensional subspaces $\{\mathbf{V}_h \subset \mathbf{V}\}$ and $\{Q_h \subset Q\}$, depending on the discretization parameter h. At this point, the Galerkin formulation of the problem reads:
find $(\mathbf{u}_h, p_h) \in \mathbf{V}_h \times Q_h$ such that:

$$\begin{cases} a_h(\mathbf{u}_h, \mathbf{u}_h, \mathbf{0}, \mathbf{v}_h) + b_h(p_h, \mathbf{v}_h) = \tilde{F}_h(\mathbf{v}_h) & \text{for all } \mathbf{v}_h \in \mathbf{V}_h, \\ -b_h(\mathbf{u}_h, q_h) = G_h(q_h) & \text{for all } q_h \in Q_h \end{cases} \tag{42}$$

3.2 Energy Balance and Species Mass Fraction equations

In the same way as for the Navier-Stokes system, we derive the weak and Galerkin formulation also for the energy balance equation and the species mass fraction equations.

3.2.1 Energy Balance

Consider the system (3): we multiply by a test function τ, regular enough and belonging to T (to be defined later), and integrate by part:

$$\int_\Omega -\mu_T \Delta T_a \tau \, d\Omega = \int_\Omega \mu_T \nabla T_a \cdot \nabla \tau \, d\Omega - \int_{\partial\Omega} \mu_T \nabla T_a \cdot \mathbf{n} \tau \, d\Gamma \quad \forall \tau \in \mathrm{T} \tag{43}$$

We then consider the boundary condition stated in (11). Imposing the Neumann condition and taking the test functions τ such that they vanish on $\{I\}$ we obtain:

$$\int_\Omega \mu_T \nabla T_a \cdot \nabla \tau \, d\Omega + \int_\Omega \mathbf{u} \cdot \nabla T_a \tau \, d\Omega = -\int_T \lambda \frac{I_{light}}{\rho_a C_p \lambda} \tau \, dT + \int_B \frac{1}{\rho_a C_p} Q_l \, \tau \, dB \quad \forall \tau \in \mathrm{T} \tag{44}$$

Moreover, as in the previous section, to deal with the non homogeneous Dirichlet boundary conditions over the surface I, we introduce a lifting operator R_{T_I}. Replacing in (44) $T_a = \dot{T}_a + R_{T_I}$ with the same steps as before we obtain the weak formulation:
find $\dot{T}_a \in \mathrm{T}$ such that

$$\int_\Omega \mu_T \nabla \dot{T}_a \cdot \nabla \tau \, d\Omega + \int_\Omega \mathbf{u} \cdot \nabla \dot{T}_a \tau \, d\Omega = F(\tau) \quad \forall \tau \in \mathrm{T} \tag{45}$$

where

$$F(\tau) = -\int_T \frac{I_{light}}{\rho_a C_p} \tau \, dT + \int_B \frac{1}{\rho_a C_p} Q_l \, \tau \, dB - \int_\Omega \mu_T \nabla R_{T_I} \cdot \nabla \tau \, d\Omega - \int_\Omega \mathbf{u} \cdot \nabla R_{T_I} \tau \, d\Omega \quad \forall \tau \in \mathrm{T}$$

and $\mathrm{T} = H^1_I(\Omega) = \{\tau \in H^1(\Omega) : \tau \,|_I = 0\}$. Taking the same triangulation $\boldsymbol{\tau}_h$ previously introduced, we can take a family of finite dimensional subspaces $\{T_h \subset \mathrm{T}\}$, and the Galerkin formulation of the problem is:
find $T_{a_h} \in \mathrm{T}_h$ such that

$$\int_\Omega \mu_T \nabla T_{a_h} \cdot \nabla \tau_h \, d\Omega + \int_\Omega \mathbf{u} \cdot \nabla T_{a_h} \tau_h \, d\Omega = F_h(\tau_h) \quad \forall \tau_h \in \mathrm{T}_h. \tag{46}$$

3.2.2 Mass Fraction

Analogously, we do the same steps for the species mass fraction equations (6). We multiply for a test function h, regular enough and null on $\{I\}$. Also in this case the diffusion coefficient is constant, leading to

$$-\int_\Omega \mathrm{div}(D_n \nabla \gamma_n) h \, d\Omega = -\int_\Omega D_n \Delta \gamma_n h \, d\Omega \tag{47}$$

we integrate by parts:

$$-\int_\Omega D_n \Delta \gamma_n h \, d\Omega = \int_\Omega D_n \nabla \gamma_n \cdot \nabla h \, d\Omega - \int_{\partial\Omega/\{I\}} D_n h \nabla \gamma_n \cdot \mathbf{n} \, d\Gamma \quad \forall h \in G. \tag{48}$$

Then, by imposing the Neumann boundary condition, we obtain:

$$\int_\Omega D_n \nabla \gamma_n \cdot \nabla h \, d\Omega + \int_\Omega \mathbf{u} \cdot \nabla \gamma_n h \, d\Omega = \int_B \frac{1}{\rho_a} S_n h \, dB \quad \forall h \in G \tag{49}$$

where $G = H^1_I(\Omega)$. Again, in order to be have the solution of the weak formulation and the test function in the same space, we introduce a lifting operator R_{γ_I}, we replace $\gamma_n = \dot{\gamma}_n + R_{\gamma_I}$ in the equation and we obtain the weak formulation:
find $\dot{\gamma}_n \in G$ such that

$$\int_\Omega D_n \nabla \dot{\gamma}_n \cdot \nabla h \, d\Omega + \int_\Omega \mathbf{u} \cdot \nabla \dot{\gamma}_n h \, d\Omega = F(h) \quad \forall h \in G, \tag{50}$$

where

$$F(h) = \int_B \frac{1}{\rho_a} S_n h \, dB - \int_\Omega \left(\mathbf{u} \cdot \nabla R_{\gamma_I} h + D_n \nabla R_{\gamma_I} \cdot \nabla h\right) d\Omega \quad \forall h \in G.$$

Considering the family of finite-dimensional subspaces $\{G_h \subset G\}$, the Galerkin formulation of the problem is:
find $\gamma_{n_h} \in G_h$ such that

$$\int_\Omega D_n \nabla \gamma_{n_h} \cdot \nabla h_h \, d\Omega + \int_\Omega \mathbf{u} \cdot \nabla \gamma_{n_h} h_h \, d\Omega = F_h(h_h) \quad \forall h_h \in G_h. \tag{51}$$

4 Numerical Implementation

In this section, the theoretical framework explained earlier is put into practice. The software employed is FreeFem++: an open-source programming language focused on solving PDEs using the finite element method (FEM). Here we provide an overview of the methodologies employed, the designed algorithms, and the computational techniques used to realize our project goals. Then, we assess the numerical convergence to validate our code.
As extensively discussed in Section 2, the examined domain is a square cell with edge $L = 1m$ with 1 lettuce plant modeled with the *Big-Leaf* approximation. An air flow is imposed across the y-direction, in the upper face of the cell the presence of the LED lights is considered. To avoid further complicating our already substantial model, the flow is assumed to be laminar and the value of the air viscosity, although nonphysical, is fixed at $\mu = 10^{-1}$. Actually, the correct physical value for μ is of the order of 10^{-5}, but we were not able to adopt a lower value than 10^{-1} due to computational heaviness issues. Indeed, lower values of μ yield to higher values for Reynolds number, leading to turbulence effect that cannot be handled without a turbulence model.
We simulate the growth of the lettuce for a period of 20 days, through a loop in time in which, at each iteration, all the balance equations are performed. First, the energy balance and species mass fraction equations are solved, consequently the dry weight is calculated. In the end, LAI and ET are computed.
On the other hand, since the fluid domain does not change in time, the Navier-Stokes system is solved only once before entering the time loop.
As before, we analyze the numerical implementation of each system of equations separately.

4.1 Newton's method applied to NS equations

We start focusing on finite element implementation of the problem (42).
Under suggestion of *Agricola Moderna*, we set an inlet flow $U = [0, 0.3, 0]^T\ ms^{-1}$, which is a realistic physical value. As discussed in section 2.1.3, no-slip conditions are imposed in the lateral faces and homogeneous Neumann boundary condition at the outlet face. To treat the non-linearity and solve the system of equations, we employed the Newton's method ([8]). In accordance with FreeFem's documentation[5], Newton's algorithm applied to (42) reads:
find $(\mathbf{u}_{n+1}, p_{n+1}) \in \mathbf{V} \times Q$ such that:

$$\begin{cases} a(\mathbf{u}_{n+1}, \mathbf{u}_n, \mathbf{u}_n, \mathbf{v}) + b(p_{n+1}, \mathbf{v}) = -(\mathbf{u}_n \cdot \nabla)\mathbf{u}_n\mathbf{v} + \tilde{F}(\mathbf{v}) \\ -b(\mathbf{u}_{n+1}, q) = G(q) \end{cases} \tag{52}$$

for all $\mathbf{v} \in \mathbf{V}$ and $q \in Q$ [6]. As initial guess $(\mathbf{u}_0, p_0)$ of the method we employ the finite element approximation solution to incompressible Stokes equations:

$$\begin{cases} a(\mathbf{u}^{(0)}, \mathbf{0}, \mathbf{0}, \mathbf{v}) + b(p^{(0)}, \mathbf{v}) = \tilde{F}(\mathbf{v}) \\ -b(\mathbf{u}^{(0)}, q) = G(q). \end{cases} \tag{53}$$

In order to be able to guarantee the existence of an unique solution of (53), we want to apply Theorem 16.3 in [9]. For this reason, as finite dimensional subspaces we choose the pair $\mathbb{P}_2 - \mathbb{P}_1$ (continuous piecewise quadratic velocities and continuous piecewise linear pressure). Hence, considering the triangulation τ_h, we define:

$$\mathbf{V}_h = \{\mathbf{v}_h \in \mathbf{V} : \mathbf{v}_h|_k \in (\mathbb{P}_2)^3 \quad \forall k \in \tau_h\}$$
$$Q_h = \{q_h \in Q : q_h|_k \in (\mathbb{P}_1) \quad \forall k \in \tau_h\}.$$

Indeed, $\mathbb{P}_2 - \mathbb{P}_1$ is the smallest degree representative of Taylor-Hood elements $\mathbb{P}_k - \mathbb{P}_{k-1}, k \geq 2$ (continuous velocities and continuous pressure) that observe the *inf-sup* condition.
We develop the algorithm with a tolerance equal to 10^{-6} and maximum number of iterations 300.

4.2 Energy Balance and Species Mass Fraction equations

We proceed with the implementation of the energy balance and species mass fraction equations. Since we are dealing with two diffusion-advection equation, we consider the general problem introduced in *Remark 1*, and we apply it to the two problems (46) and (51). In particular, we note that in both cases the advection term dominates over the diffusion one. This makes the Galerkin method more prone to oscillations and instabilities. A plausible solution is to stabilize the problem by adding a further term to the Galerkin approximation. The considered general problem is therefore:
find $u_h \in \mathrm{V}_h$ such that

$$\int_\Omega \mu \nabla u_h \cdot \nabla \psi_h \, d\Omega + \int_\Omega \mathbf{b} \cdot \nabla u_h \psi_h \, d\Omega + \mathcal{L}_h(u_h, f; \psi_h) = F_h(\psi_h) \quad \forall \psi_h \in \mathrm{V}_h \tag{54}$$

[7]

for a suitable form $\mathcal{L}_h$ satisfying

$$\mathcal{L}_h(u, f; \psi_h) = 0 \quad \forall \psi_h \in \mathrm{V}_h. \tag{55}$$

We choose the suitable $\mathcal{L}_h$ by implementing the Streamline Upwind Petrov-Galerkin (SUPG) method, which is a strongly consistent method, namely we set:

$$\mathcal{L}_h(u_h, f; \psi_h) = \sum_K \left(Lu_h - f, \boldsymbol{\tau}_K \mathcal{S}(\psi_h)\right)_{L^2(K)}, \tag{56}$$

[5] https://doc.freefem.org/tutorials/navierStokesNewton.html
[6] Note that we have replaced $\mathbf{u}_h$, $\mathbf{v}_h$, p_h and q_h with respectively $\mathbf{u}$, $\mathbf{v}$, p and q to avoid heavy notation.
[7] Note that here μ refers to the generic diffusion coefficient and u_h to a generic discretized unknown.

where K are the mesh element of the triangulation, $(u,v)_{L^2(K)} = \int_K uv\, dK$, and $\boldsymbol{\tau}_K$ is a stabilization parameter to be determined. We set

$$\mathcal{S}(\psi_h) = L_{SS}\psi_h, \tag{57}$$

where L_{SS} is the skew-symmetric part of the operator L, defined as in (9). Concerning the stabilization term $\boldsymbol{\tau}_K$, we choose:

$$\boldsymbol{\tau}_K(\mathbf{x}) = \frac{h_K}{2|\mathbf{b}(\mathbf{x})|}\xi(\mathbb{P}e_K) \quad \forall \mathbf{x} \in K,\, \forall K \in \boldsymbol{\tau}_h, \tag{58}$$

where $h_K = \max\{\text{diam}(K) | K \in \boldsymbol{\tau}_h\}$ and

$$\mathbb{P}e_K(\mathbf{x}) = \frac{|\mathbf{b}(\mathbf{x})|h_K}{2\mu} \quad \forall \mathbf{x} \in K,\, \forall K \in \boldsymbol{\tau}_h \tag{59}$$

is the local Péclet number, and the upwind function $\xi(\cdot)$ is

$$\xi(\theta) = \coth(\theta) - 1/\theta, \quad \theta > 0. \tag{60}$$

For our equations, it happens that $\mathbb{P}e_K >> 1$, namely $\mathbb{P}e_K \sim 10^3$, which implies $\xi(\mathbb{P}e_K) \sim 1$. Moreover, we have that the advection term $\mathbf{b}$ is equal to the velocity $\mathbf{u}$, thus $\boldsymbol{\tau}_K$ becomes

$$\boldsymbol{\tau}_K(\mathbf{x}) = \frac{h_K}{2|\mathbf{u}(\mathbf{x})|} \quad \forall \mathbf{x} \in K,\, \forall K \in \boldsymbol{\tau}_h. \tag{61}$$

4.2.1 Energy balance

For the energy balance, we start from (46) and, since the temperature is a scalar quantity, we set $\mathrm{T}_h = \mathbb{P}_1$ to be coherent with what done before. We considered the stabilized problem:
find $T_{a_h} \in \mathrm{T}_h$ such that

$$\int_\Omega \mu_T \nabla T_{a_h} \cdot \nabla \tau_h \, d\Omega + \int_\Omega \mathbf{u} \cdot \nabla T_{a_h} \tau_h \, d\Omega + \mathcal{L}_h(T_{a_h}; \tau_h) = F_h(\tau_h), \quad \forall \tau_h \in \mathrm{T}_h \tag{62}$$

where we have considered $\mu = \mu_T$, F_h is defined in (46) and:

$$\mathcal{L}_h(T_{a_h}; \tau_h) = \sum_K (LT_{a_h}, \boldsymbol{\tau}_K L_{SS}\tau_h)_{L^2(K)} \tag{63}$$

In this case, the skew-symmetric operator turns out to be $L_{SS}\tau_h = \mathbf{u} \cdot \nabla \tau_h$. Moreover, using $\mathbb{P}_1$ finite elements, we have that $-\Delta T_{a_h}|_K = 0 \, \forall K \in \boldsymbol{\tau}_h$. Thus, the equation can be written as:

$$\int_\Omega \mu_T \nabla T_{a_h} \cdot \nabla \tau_h \, d\Omega + \int_\Omega \mathbf{u} \cdot \nabla T_{a_h} \tau_h \, d\Omega + \sum_K \int_K \boldsymbol{\tau}_K (\mathbf{u} \cdot \nabla T_{a_h})(\mathbf{u} \cdot \nabla \tau_h) = F_h(\tau_h), \quad \forall \tau_h \in \mathrm{T}_h \tag{64}$$

The PDE is then solved with the specific built-in function `problem` of FreeFem++.

4.2.2 Species Mass Fraction equations

In the same way, for the species mass fraction balance (51), we choose $G_h = \mathbb{P}_1$, and we add the stabilization term using SUPG method. With the same reasoning as before, the equation to solve becomes:

$$\int_\Omega D_n \nabla \gamma_{n_h} \cdot \nabla h_h \, d\Omega + \int_\Omega \mathbf{u} \cdot \nabla \gamma_{n_h} h_h \, d\Omega + \sum_K \int_K \boldsymbol{\tau}_K (\mathbf{u} \cdot \nabla \gamma_{n_h})(\mathbf{u} \cdot \nabla h_h) = F_h(h_h), \quad \forall h_h \in G_h \tag{65}$$

where we have considered that $\mu = D_n$ and F_h defined in (51). We solve it with the function `problem`. In particular, the boundary terms S_{H_2O} and S_{CO_2} are imposed to zero in the first iteration, then they are obtained as feedback from the photosynthesis equation (20) (see Remark 2).

Remark 4. *Solving numerically* (65) *we obtain a vector, where CO_2 and H_2O mass fraction values are registered punctually. Since the solution of the ODE system* (13) *requires scalar values, we, then, approximate them with an integral mean over the specific region of interest, which depending on the case could be the exchange region or the area out of it.*

4.3 Dry weight equations

As discuss in the Section 2.2, the dry weight equations form a ODE system; since in `FreeFem++` software it is not provided any pre-implemented method to solve that type of equations, we developed the code from scratch. We choose to solve the system employing the Crank-Nicolson (CN) method. It is a well-known implicit, second-order method in time, which is unconditionally stable for every Δt and with accuracy $\mathcal{O}(\Delta t^2)$, where Δt is the time-step. The system is then solved by the fixed point technique with tolerance 10^{-6} and maximum number of iterations 100. The initial dry weight values provided by *Agricola Moderna* are:

$$\begin{cases} X_{\text{nsdw}} = 6.75 \cdot 10^{-5}\ g/m^2; & \text{non-structural dry weight} \\ X_{\text{sdw}} = 2.25 \cdot 10^{-5}\ g/m^2; & \text{structural dry weight} \end{cases}$$

In particular, as explained in section 2.2.3, the result value of the gross canopy photosynthesis f_{phot} is used as feedback for the source terms S_{H_2O} and S_{CO_2} in (51).

4.4 Crop energy balance

At the end of every time-loop iteration, we can easily solve the system (25), computing the heat exchange between the plant and the surrounding environment and, finally, through relation (29), we are to able to obtain the desired evapotranspiration index, ET.

Remark 5. *We remark again that the latent heat exchange, Q_l, is used as feedback for the source term in the energy balance equation* (44).

4.5 Grid study

As a way to assess the independence of the numerical results from the dimension of the grid, we perform, here, a grid study. Five grid numbers, ranging from $10 \times 10 \times 10$ (coarse) to $30 \times 30 \times 30$ (fine), are used to study the baseline case. In order to align the complexity intrinsic of the problem and the numerical one, the parameters related to the Reynolds number are all set to 1. We continue by selecting a target parameter and verifying that, as the number per side of mesh elements N increases, the value of interest begins to become constant, i.e. independent of the grid size.

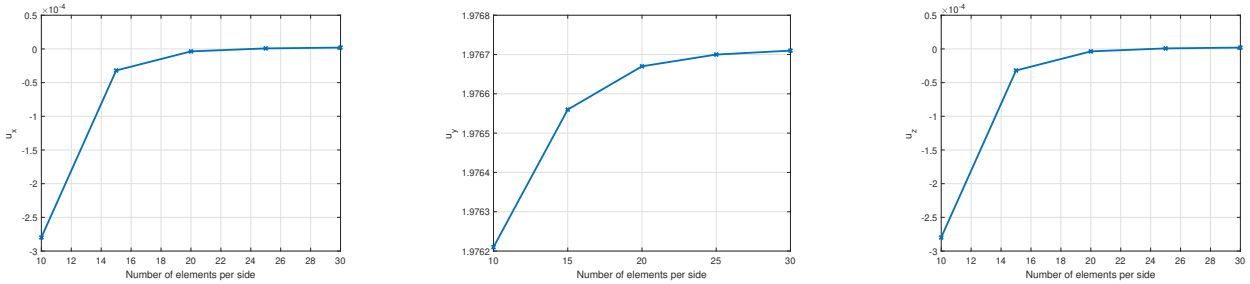

(a) Velocity along x-direction (b) Velocity along y-direction (c) Velocity along z-direction

Figure 1: Velocity grid refinement test

In the case of Navier-Stokes equations, the target parameter is the velocity $\mathbf{u}$ along x, y and z directions in the center of the cell. As shown in Figure 1, choosing at least $N = 20$ elements for each edge, the velocity results to be almost constant and so independent of the mesh.

Considering the energy balance and the mass fraction equations, we have that most of the variations in T, H_2O and CO_2 occur in a neighborhood the upper and lower boundary faces, respectively, due to the Neumann BCs. For this reason, the target parameter is chosen to be the value of the temperature in the middle of the upper face and the value of the concentrations of H_2O and CO_2 in the middle of the lower face.
As we can observe from the plots in Figure 2, we do not have the same behaviour of the velocity, but,

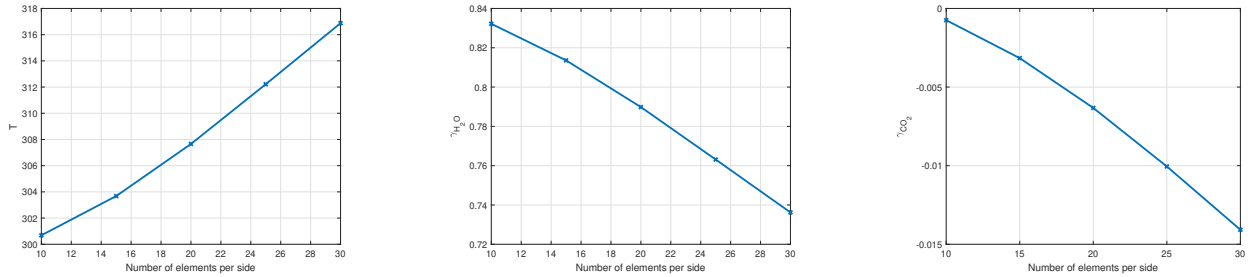

(a) Temperature grid refinement (b) H_2O grid refinement (c) CO_2 grid refinement

Figure 2: Energy balance and mass fraction grid refinement test

on the contrary, the convergence state is not reached at all, since the trend is still increasing for the temperature, Figure 2a, and decreasing for H_2O, Figure 2b, and for CO_2, Figure 2c. Therefore a run with greater meshes (> 30 elements per side) should be appropriate to established when the constant region of the plot becomes. Nevertheless, for computational reasons, we decide not to proceed further with the study of a finer mesh, and we select the finest as the best.

Therefore, balancing between the accuracy of the simulation results and the computation costs, we decide to proceed on working with $N = 30$.

5 Results

The aim of our project is to compute the evolution in time of the evapotranspiration mass rate, ET, along with the growth of a lettuce crop. This would be highly beneficial to *Agricola Moderna*, as it would enable the optimization of their energy consumption, thereby significantly reducing waste and enhancing overall efficiency.
To achieve this result, we developed a model that couples the fluid dynamics of the air flow [1] with the crops growth [2]-[3]. In this section, we present the main results obtained from our work. As for the previous sections, we proceed with a separate analysis of the different parts of the model and, finally, we present a general overview. To visualize the obtained solutions, we employ the software ParaView and MATLAB.

5.1 Newton Navier-Stokes

As usual, we start analyzing the Navier-Stokes equations, as they are the starting point of our model. To assess the quality of the results, we first plot the computed quantity inside the domain. This is a theory related control: since we are considering a laminar, steady state and incompressible flow between two plates, we are under the assumptions of the Poiseuille plane flow; therefore, the expected behaviour is well-known. For what concerns the velocity, the expected result is a parabolic profile, with the higher value reached in correspondence of the center of the cell. As we can see in Figure 3, our simulation provides the expected result.
Even if is less relevant for our overall model, we also examine the behavior of the pressure, to make sure that our solution is correct. Its results are visualized in Figure 4. We can see that the pressure correctly decreases from the inlet (on the left) to the outlet (on the right), highlighting the presence of a negative pressure gradient, typical of the Poiseuille flow. The small high-pressure regions at the inlet are expected boundary effects: the inlet velocity is uniform, not parabolic, hence close to the walls the velocity must decrease extremely quickly to satisfy no-slip conditions.
We proceed with a deeper analysis of the velocity results, as it is of primary interest in our model. We decide to compute the error of the solution in relation to the mesh size. Since we do not have an analytical solution, to test the accuracy of the code we decide to take as benchmark the one obtained using the finer mesh at our disposal: the one with $N = 30$. We compute the error as the H^1-norm of the difference between the current and the benchmark result, divided by the H^1-norm of the latter.

(a) Lateral view of the velocity field on the median slice.

(b) Velocity parabolic profiles at a cross section.

Figure 3: Visualization of the velocity field inside the cell with the inflow coming from the left.

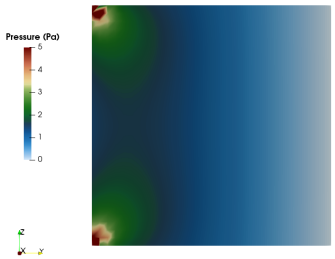

Figure 4: Visualization of the pressure values inside the cell from a lateral view.

We cannot use an a-priori estimate to assess the correctness of the error trend, since we do not have an exact solution. Thus, we just plot it against h and h^2, in order to have a comparison term, that can give a hint about the exactness of the solution. As shown in Figure 5, we can observe that the error

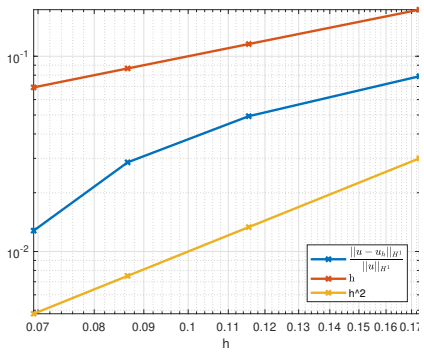

Figure 5: Velocity error against grid size.

decreases as the mesh size increases, with a behaviour between the linear and the quadratic trend.

5.2 Energy Balance

Now, we consider the energy balance equation. The results shown in Figure 6a and in Figure 6b highlight that the temperature remains almost uniform in the inner region of the cell. Close to the top boundary, we can notice the presence of the LED, imposed a heat flux entering the cell. Moreover, notice that advancing in time, in the lower part a sink effect arises, as already anticipated in Remark 2. Indeed, as the days go by, the crop grows and the effect of transpiration becomes more and more relevant: this increases the heat flux toward the lettuce, resulting in a lowering of the temperature

in the surrounding area. The higher and lower temperature zones are more thick close to the outlet because of the velocity profile: advection dominates over diffusion and so also the heat fluxes at the boundaries feel the effect of transport.

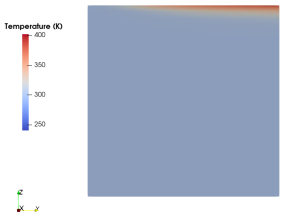

(a) Temperature on the first day of the simulation

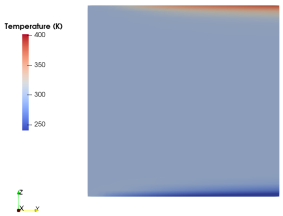

(b) Temperature at the end of the crop growth

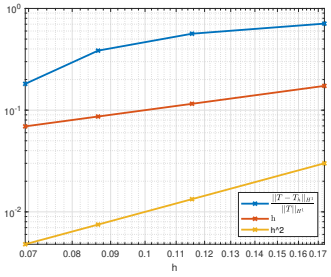

(c) Temperature error plot

Figure 6: Visualization of the temperature (in K) inside the cell (on the left and centre) and temperature error against grid size (on the right).

As reported in Figure 6c, we observe that, also in this case, the error decreases as the mesh size increases, and it has a behaviour between linear and quadratic trend.

5.3 Species Mass Fraction

Now, we analyse the species mass fraction γ_{CO_2} and γ_{H_2O}. In Figure 7a, Figure 7b, Figure 8a, Figure 8b we can see that, as expected, the values of the CO_2 and H_2O are almost uniform across the cell. As it happens for the temperature, also in this case the flux at the lower boundary increases as the crop grows. In particular, in agreement with the photosynthesis reaction, the crop absorbs CO_2 and H_2O from the environment: the more mass the lettuce gain, the more it is able to photosynthesize. Moreover, in agreement with our expectation, also in this plots it is possible to see that the thickness of the low-concentration layer increases close to the outlet face. This transport effect is expected as advection dominates over diffusion.

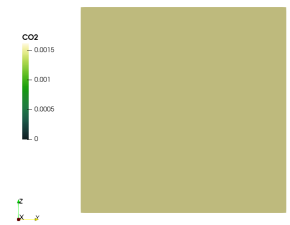

(a) CO_2 concentration on the first day of the simulation

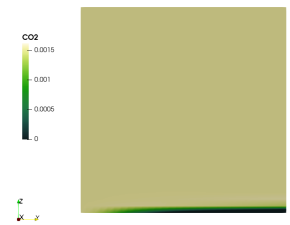

(b) CO_2 concentration at the end of the crop growth

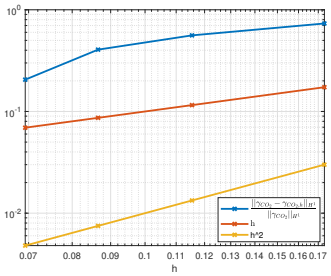

(c) Error of the H_2O concentration

Figure 7: Visualization of the CO_2 concentration at the beginning (on the left) and at the end (in the middle) of the simulation and CO_2 concentration error against grid size (on the right).

Moreover, looking at the error plot shown in Figure 7c and Figure 8c, we observe that we have the same behavior of the temperature.

5.4 Lettuce crop growth

As it was explained in section 2.2, the lettuce crop growth is quantified through the amount of dry weight of the canopy. We analyse the results obtained over the entire duration of the simulation, i.e. 20 days. The results are reported in Figure 9. The crop shows a growth behavior in time, as

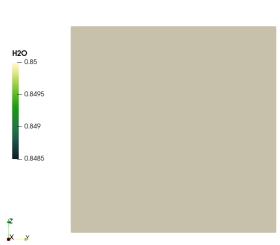

(a) H_2O concentration on the first day of the simulation

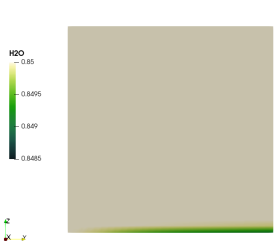

(b) H_2O concentration at the end of the crop growth

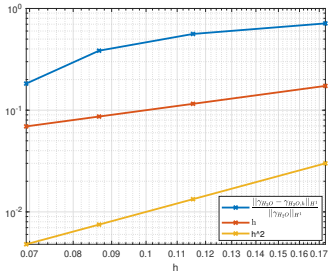

(c) Error of the H_2O concentration

Figure 8: Visualization of the H_2O concentration at the beginning (on the left) and at the end (in the middle) of the simulation H_2O concentration error against grid size (on the right).

obviously we were expecting. The numerical value of the total weight is also reasonable. However, the value obtained is a bit lower than the expected one provided by *Agricola Moderna*. Nevertheless, accounted that our model involves several simplifying assumptions, we can confidently state that it yields satisfactory results.

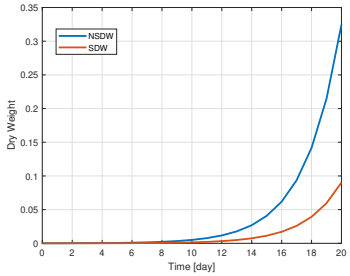

Figure 9: Growth of a lettuce crop

5.5 Evapotranspiration rate

The ultimate goal of our analysis is the computation of the evapotranspiration rate evolution in time. As we can see from figure 10, the ET remains almost equal zero up to the 15^{th} day. After that it shows the expected exponential growth. Again, as it was for the canopy dry weight, the values obtained are not exactly the expected ones. However, they are reasonable enough under our assumptions; also, the exponential growth behavior has been successfully achieved, hence we can be satisfied.
The low values we obtained are due to the difference $\gamma_{H_2O,c} - \gamma_{H_2O,a}$ at the numerator (see eq. (29)). In fact, in our model this difference only depends on the intensity of the H_2O mass fluxes towards the canopy, that are necessary to photosynthesize. Before the very last days, the dry weight is not large enough to make the photosynthesis to have a relevant impact on such fluxes. Hence, before day 15, the H_2O concentration is almost uniform in the whole domain, including the lower layer.

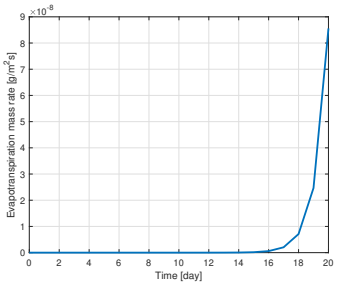

Figure 10: Evapotranspiration mass rate evolution

6 Conclusion

In this few pages, we have proposed our model devoted to compute the evolution in time of the evapotranspiration rate of a lettuce crop, in fashion that it can be an important tool for *Agricola Moderna* to enhance a better usage of their energy, so as to avoid waste.
We started by carefully reading three different papers about three different aspects of the vertical farm environment: one was related to the consume of energy inside a cell [1], one was related to the computation of growth evolution of a lettuce crop [2] and the last one was dedicated to the analysis of the fluid-dynamics inside a cell [3].
Then, we proceeded by developing a for loop structure, simulating 20 days, where, starting from the fluid-dynamics equation (*Navier-Stokes, Energy Balance, Species Mass Fraction*) and solving and ODEs system for the growth of a lettuce crop, we estimated a measure for the evapotranspiration mass rate, ET. We highlight that some of the results obtained at each iteration are used as feedback. This model was developed from scratch, based only on previous literature that is listed in the bibliography below. For this reason, we are highly satisfied with our results. Moreover, since this is a brand new model, it is suitable for being adopted as a starting point for further developments. For these reasons, here we point out some features that might be implemented to improve the accuracy and the reliability of the output estimates:

- The actual viscosity of air μ is of the order of 10^{-5} $[kg\,m^{-1}\,s^{-1}]$. This means that, coupled with a realistic dimension for the cell, the resulting flow will be turbulent. Therefore, it would be a nice feature to add a turbulence model to the Navier-Stokes solution, so that the model can run with realistic values.

- The crop influence over the energy balance and mass fraction equations appears as a boundary conditions. An improvement would be to properly insert it inside the domain by shaping it such that it changes at each iteration in time as the crop grows. Of course this advanced feature yields more turbulence to the flow, so it is recommended to first implement a turbulence model as discussed right above.

- As known in reality, a crop undergoes to a night-day cycle. Nevertheless, for the sake of simplicity, we assumed that the lights in the cell are always on. Thus, one next move could be to implement an algorithm that takes into account the fact that for 8 hours per day the lights are turned off.

- For the solution of the ODEs system we have used a Crank-Nicholson method, which is known to be unconditionally stable, but it can undergo to oscillations. Thus, a further development could be to substitute it with multi-steps schemes, such as Runge-Kutta, BDF or Adams methods, which can result less subjected to oscillations and more precise in the solution.

- The paper [2] from which we adapted the model for the crop dry weight growth in time, was written in 1992. The model overall works quite well, but in literature it is possible to find more modern, accurate, temperature and weight sensitive ways to compute the leaf area index with respect to the formula 22. Newer models include correction parameters obtained empirically from observed data. Other models exploit also image analysis to measure the LAI.

References

[1] B. Naranjani, Z. Najafianashrafi, C. Pascual, I. Agulto, and A. Chuang. Computational analysis of the environment in an indoor vertical farming system. *International Journal of Heat and Mass Transfer*, 186:1–12, 2022.

[2] E. J. Van Henten. Validation of a dynamic lettuce growth model for greenhouse climate control. *Agricultural Systems*, 45:55–72, 1994.

[3] Luuk Graamans et al. Plant factories; crop transpiration and energy balance. *Agricultural Systems*, 153:138–147, 2017.

[4] W. J. Massman. A review of the molecular diffusivities of h2o, co2, ch4, co, o3, so2, nh3, n2o, no, and no2 in air, o2 and n2 near stp. *Atmospheric Environment*, 32:1111—1127, 1998.

[5] Kleber C. Mundim, Solange Baraldi, Hugo G. Machado, and Fernando M.C. Vieira. Temperature coefficient (q10) and its applications in biological systems: Beyond the arrhenius theory. *Ecological Modelling*, 431:109–127, 2020.

[6] FAO Food and Agriculture Organization of the United Nations. Crop evapotranspiration - guidelines for computing crop water requirements. *FAO Irrigation and drainage paper 56*, 1998, Rome.

[7] B.R. Munson, D.F. Young, T.H. Okiishi, and W.W. Huebsch. *Fundamentals of Fluid Mechanics*. Wiley, 2009.

[8] Sang Dong Kim, Yong Hun Lee, and Byeong Chun Shin. Newton's method for the navier-stokes equations with finite-element initial guess of stokes equations. *Computers & Mathematics with Applications*, 51:805–816, March 2006.

[9] Alfio Quarteroni. *Numerical Models for Differential Problems*. Springer Milano, 2012.